S1 OH reaction rates

Ozonolysis of olefins is known to produce OH as a product of Criegee intermediate decomposition. To minimize the role of OH in oxidizing β-caryophyllene, 2-butanol was used as an OH scavenger.[1] The reaction rate of the OH with 2-butanol can be determined using eq S1:

$$R_{2-but} = k_{2-but}[OH][2-but], \text{ (S1)}$$

where R is the reaction rate, k is the rate constant and [OH] and [2-but] are the concentrations on OH radicals and 2-butanol, respectively. The reactions rate of the OH radicals with β-caryophyllene can be determined using eq S2:

$$R_{\beta-car} = k_{\beta-car}[OH][\beta-car], \text{ (S2)}$$

Where [β-car] is the concentration of β-caryophyllene. Using the reaction rates of the two competing reactions, the percentage of OH radicals scavenged by 2-butanol can be calculated (eq S3):

$$\%\, Scavenged = \frac{R_{2-but}}{R_{2-but} + R_{\beta-car}} \times 100, \text{ (S3)}$$

A rate constant of 1.97×10^{-10} cm^3 $molecule^{-1}s^{-1}$ was used for the reaction between β-caryophyllene and OH.[2] A rate constant of 8.1×10^{-12} cm^3 $molecule^{-1}s^{-1}$ was used for the reaction between 2-butanol and OH.[3] The % scavenged is calculated to be ~84%, indicating that the majority of the OH radicals are scavenged by the reactions with 2-butanol.

S2 Mixing times of water within the SOA

Mixing times of water within the SOA ($\tau_{mix,H2O}$) were calculated using the following equation:[4]

$$\tau_{mix,H2O} = \frac{d_p^2}{4\pi^2 D_{H2O}}, \text{ (S3)}$$

where d_p is the diameter of the SOA particle used in the poke-flow experiments, and D_{H2O} is the diffusion coefficient of water within the SOA. The mixing time corresponds to the time it takes for the concentration of the water molecules at the centre of the particle exposed to a change in RH to differ from the equilibrium concentration by less than 1/e. To calculate $\tau_{mix,H2O}$ at each RH, we assumed that D_{H2O} in the SOA was the same as D_{H2O} in sucrose-water particles with an equivalent viscosity. For the viscosity of the SOA, we used the upper limit of the viscosity values reported in Fig. 4 of the main text. D_{H2O} was then calculated for the upper limits of the viscosity using the relationship between D_{H2O} and viscosity for sucrose-water particles developed by Price et al.[5] (Fig. 7 in Price et al.); values for $\tau_{mix,H2O}$ determined using this approach are listed in Table S1.

Tables and Figures

Table S1: Calculated mixing times of water within the SOA particles ($\tau_{mix,H2O}$) and experimental conditioning time for water vapor ($t_{exp,H2O}$), which corresponds to the time the SOA particles were exposed to a given relative humidity before the poke-flow experiments. Viscosities are based on the upper limits of viscosity shown in Fig. 4 of the main text. Diffusion coefficients were calculated using the relation between viscosity and diffusion coefficients in sucrose-water from Price et al. [5]. The variable d_p corresponds to the diameter of the SOA used in the poke-flow experiments.

RH	Upper limit of viscosity (Pa s)	Diffusion coefficient of water (m^2 s^{-1})	d_p (μm)	$\tau_{mix,H2O}$ (hrs)	$t_{exp,H2O}$ (hrs)	$t_{exp,H2O}$/ $\tau_{mix,H2O}$
48	$5.63x10^4$	$3.92x10^{-14}$	61-91	0.7-1.5	3-5	2.3-6.5
28	$4.98x10^5$	$1.13x10^{-14}$	42-69	1.1-3.0	5-24.5	2.1-22
15	$9.13x10^5$	$8x10^{-15}$	45-78	1.8-5.4	20	3.9-11.6
0	$2.42x10^7$	$1.24x10^{-15}$	30-60	5.3-20.7	2-22	0.18-2.3

Table S2: COMSOL parameters used when simulating the viscosity of β-caryophyllene SOA from poke-flow measurements

	Surface tension (mN m^{-1})	Slip length (m)	Density (kg m^{-3})	Contact angle (°)
Range of values	29.7 [a] -45[b]	$5x10^{-9}$-$1x10^{-6}$ [c]	990[d]	30-100[e]
Values for lower limit	29.7	$5x10^{-9}$	990	30-100
Values for upper limit	45	$1x10^{-6}$	990	30-100

[a]Lower limit of surface tension is the surface tension of liquid β-caryophyllene based on the model ACD/Labs Percepta Platform-PhysChem Module. Retrieved from Chemspider on May 15, 2019. [b]The upper limit is consistent with surface tension measurements of SOA at RH ≲65% RH and surface tensions reported for alcohols, organic acids, esters, and ketones, as well as surface tension measurements of water solutions containing SOA products.[6–9] [c]Range is based on measurements of the slip length of organic compounds and water on hydrophobic surfaces.[10,11,20–22,12–19] [d]Densities is based on measurements from Tasoglou and Pandis.[23] [d]Contact angle range is based on ranges measured in other chamber generated SOA [24–26]. Note: the simulated viscosities depend only weakly on the contact angle. Changing the contact angle by ±10% changes the simulated viscosity on average by ±15%, which is small compared to the overall uncertainties associated with the simulated viscosities.

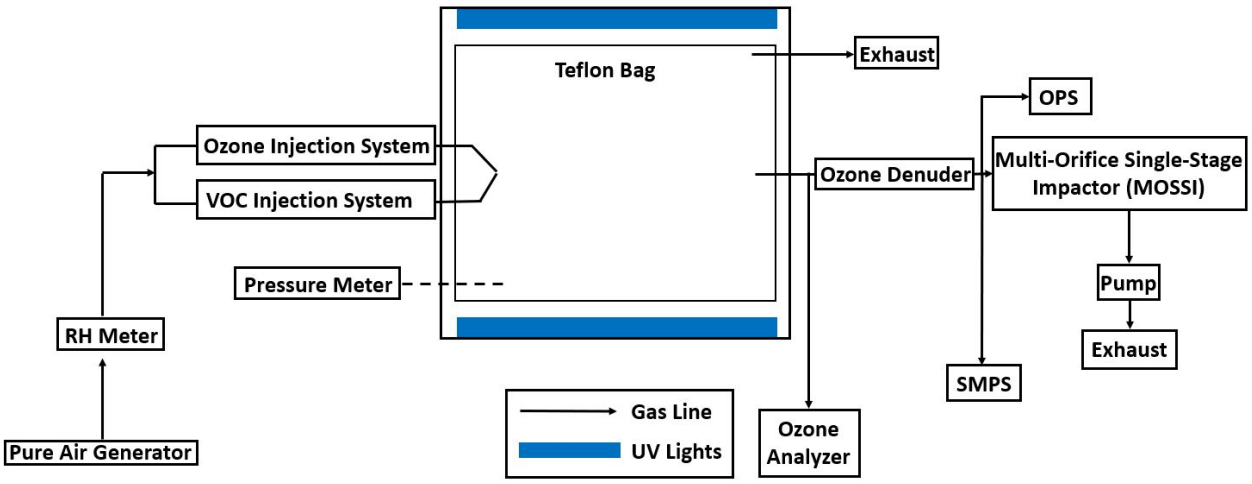

Figure S1. Schematic diagram of the UBC Environmental Chamber. There are sampling and measurement systems for ozone, temperature, relative humidity, and particle size distribution (SMPS & OPS).

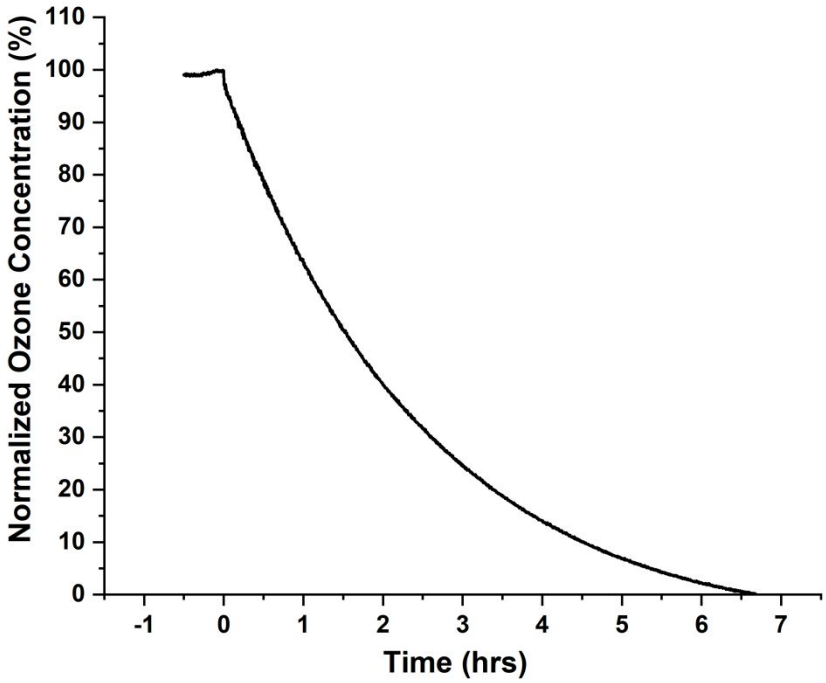

Figure S2. The change of the ozone concentration inside the chamber with respect to time. Prior to a time of 0 hrs, the ozone concentration is at a steady state of approximately 325 ppb. At 0 hrs, the ozone injection is shut off, and the concentration of ozone starts to decrease afterwards. The ozone concentration drops to half of the initial value at approximately 1.5 hours.

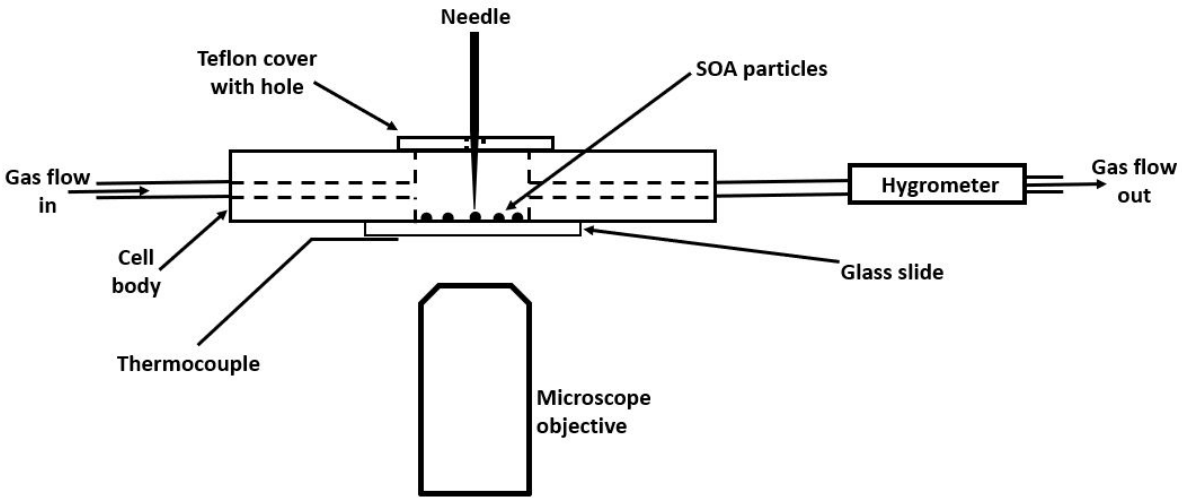

Figure S3. Diagram of the poke-flow experimental set-up.

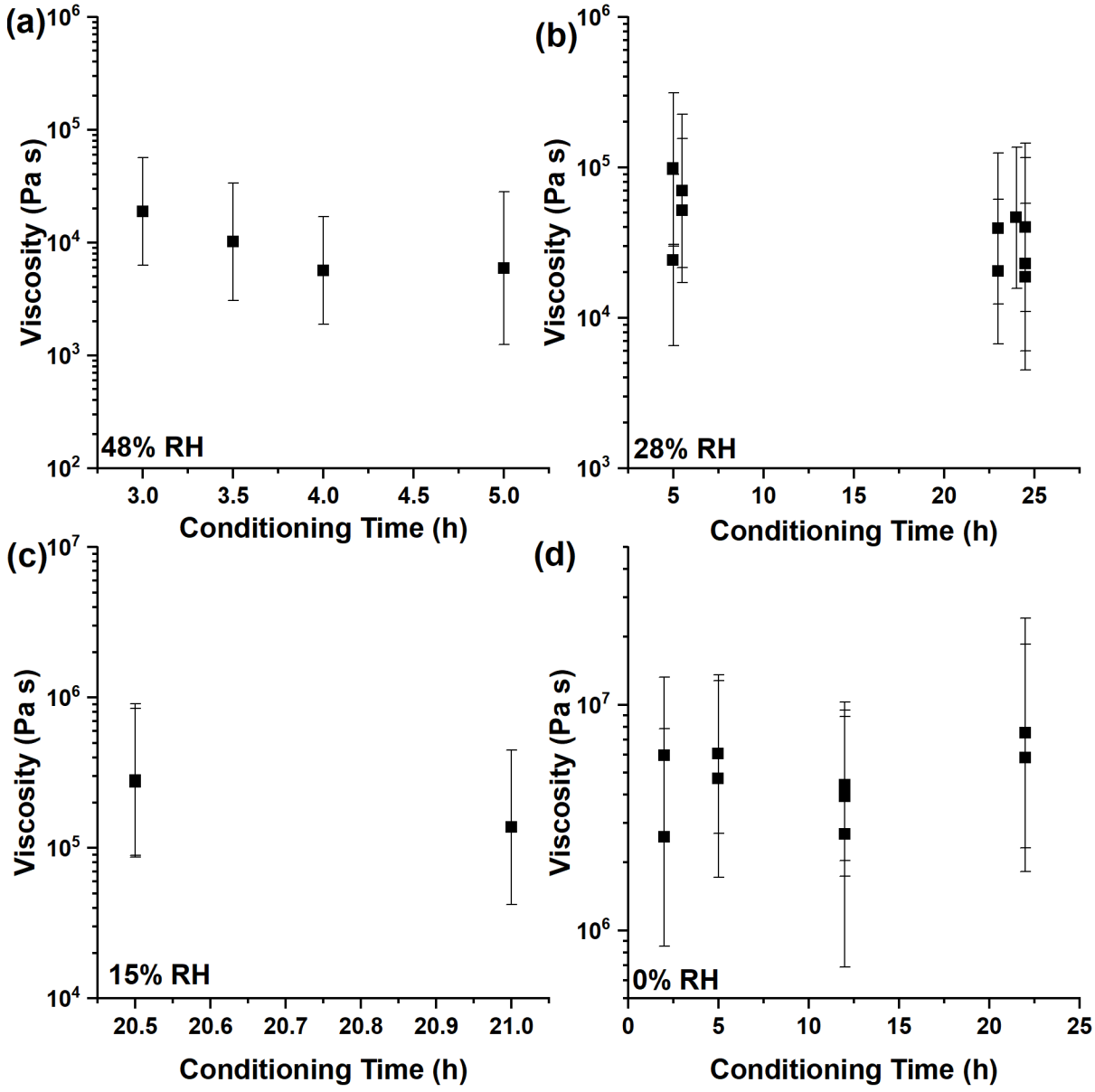

Figure S4. Viscosities as a function of particle conditioning time to the surrounding RH. Measurements were taken at RHs values of 48% in panel (a), 28% in panel (b), 15% in panel (c), and 0% in panel (d).

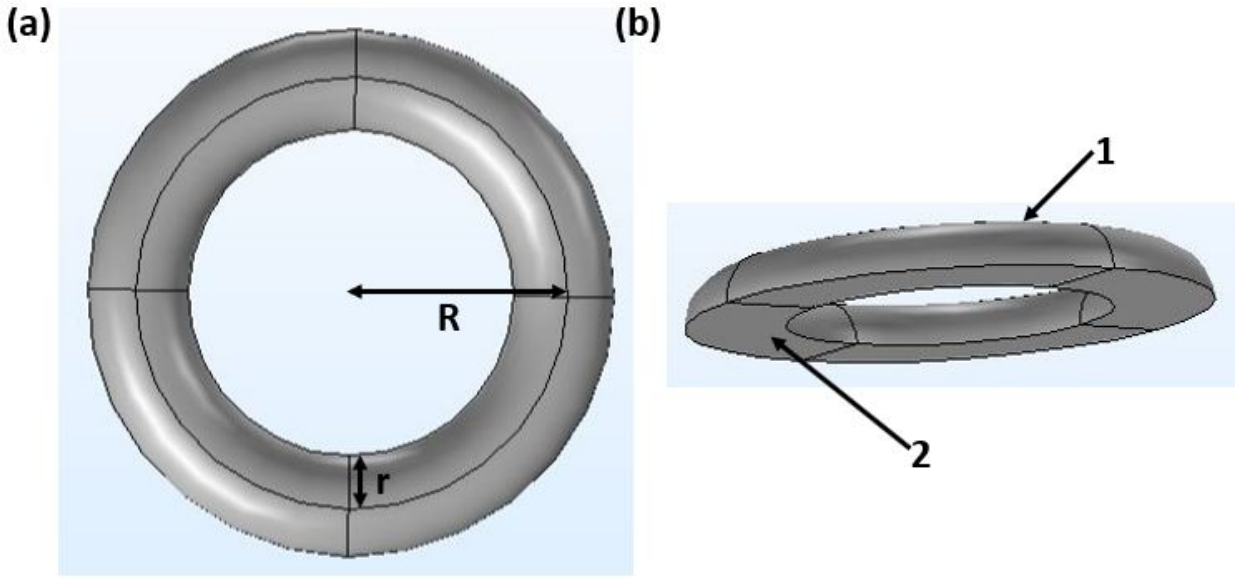

Figure S5. Geometry of the half-torus model used to simulate viscosity for the poke-flow experiments. Panel (a) shows the top view where R and r are the dimensions used to define the half-torus, and panel (b) shows a side view. In panel (b) surface 1 corresponds to the fluid-air interface, which can freely deform in all dimensions, and surface 2 corresponds to the fluid-substrate interface which can only deform parallel to the substrate surface.

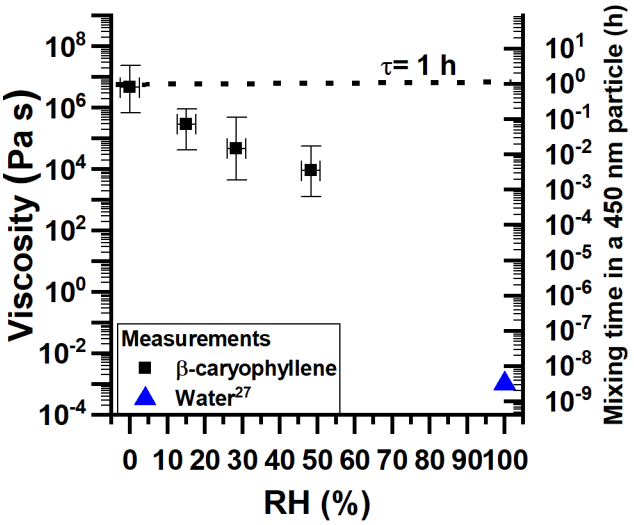

Figure S6. Viscosities of β-caryophyllene SOA and calculated mixing times within a 450 nm β-caryophyllene SOA particle. The y-error bars correspond to the upper and lower limits of viscosity from the measurements. The x-error bars correspond to uncertainties in the RH measurements. The horizontal line corresponds to a mixing time of 1 hr. The viscosity of water was taken from Crittenden et al.[27].

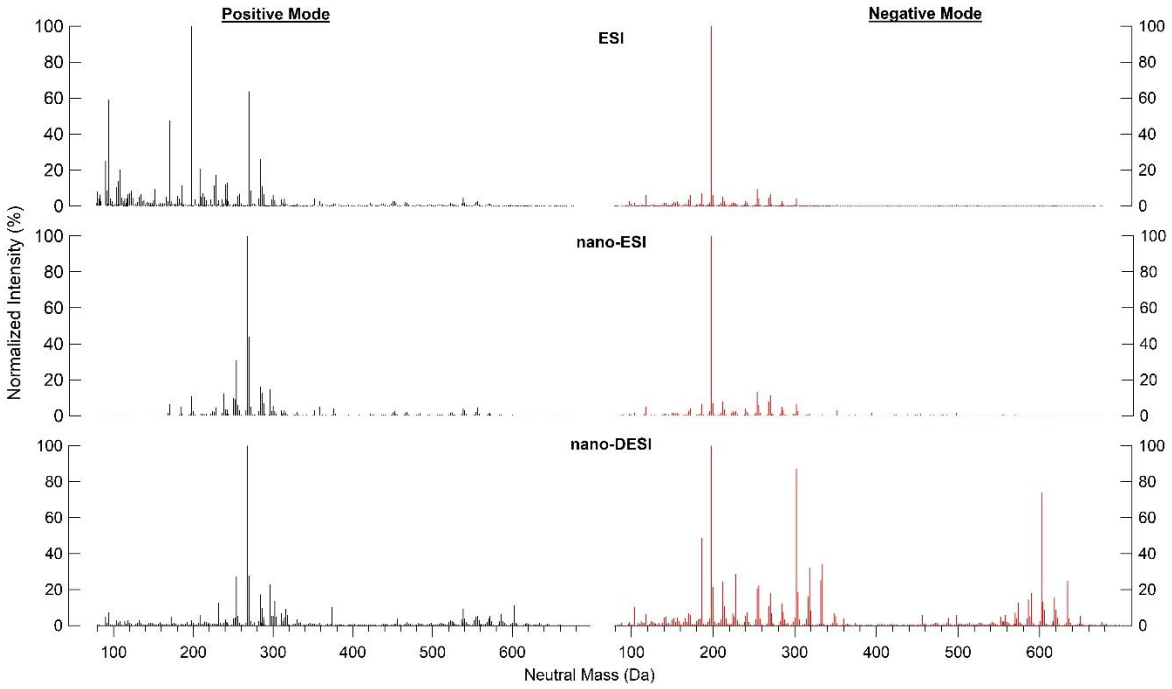

Figure S7. High-resolution mass spectrometry data taken with ESI, nano-ESI, and nano-DESI ionization sources in both positive and negative mode. The intensities were normalized to the largest peak within each ionization mode.

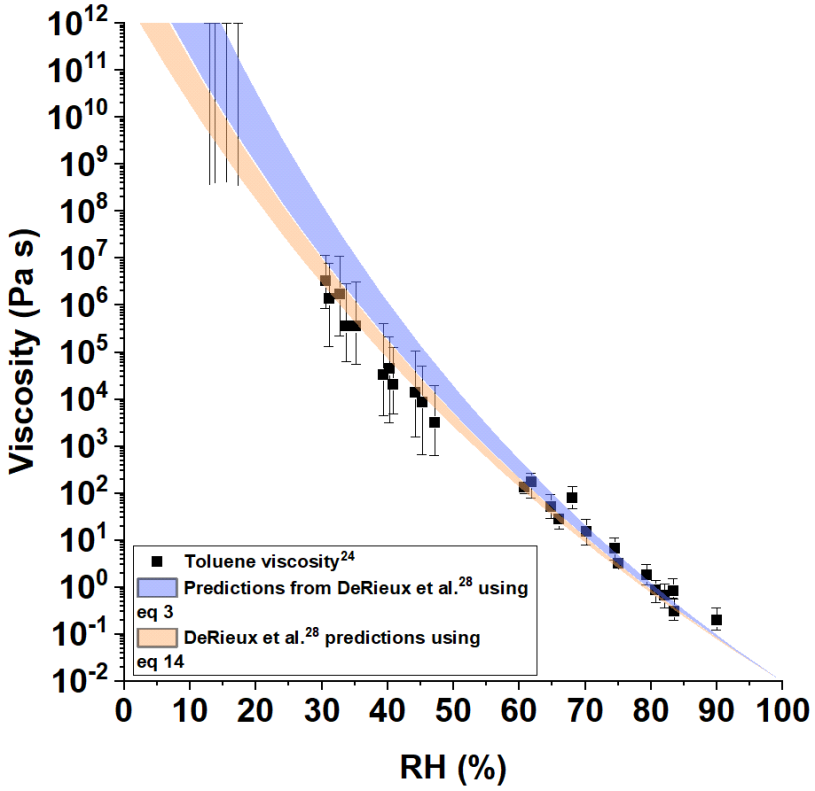

Figure S8. Toluene SOA viscosity as a function of RH. The y-error bars correspond to the upper and lower limits of viscosity from the measurements. Shown in blue are the viscosity predictions based on nano-DESI positive mode mass spectrometry results from DeRieux et al. [28] where it was assumed that the weight fraction of individual compounds was proportional to the mass spectrum signal intensity (eq 3). Shown in orange are the viscosity predictions from DeRieux et al. [28] where a relation between weight fraction and intensity given in eq 14 of the main text was assumed. The shaded regions were calculated from nano-DESI mass spectrometry data collected at high and low RH separately.[29]

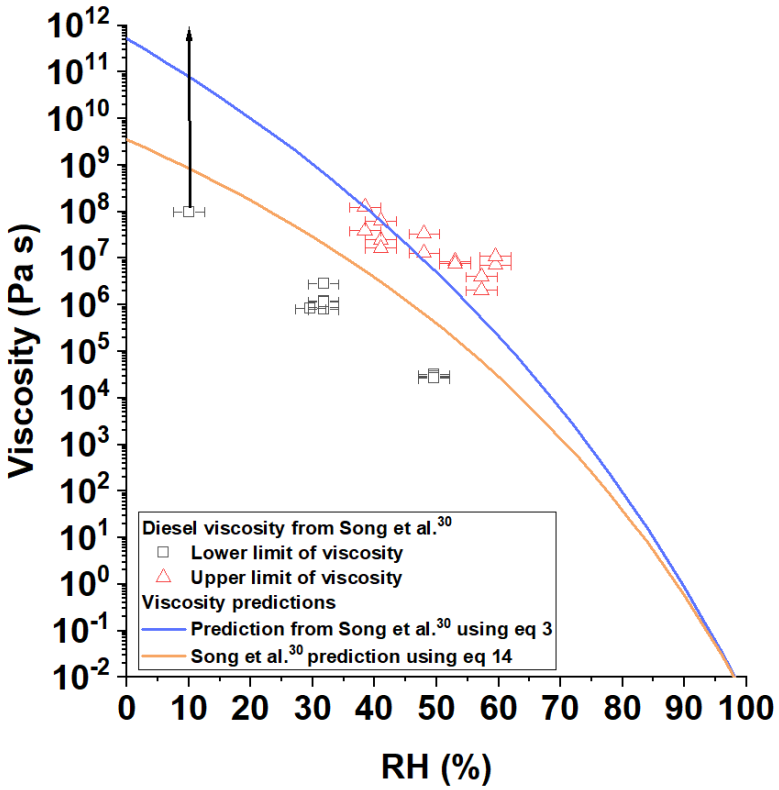

Figure S9. Diesel fuel vapour SOA viscosities as a function of RH. The x-error bars correspond to uncertainties in the RH measurements and the y-error bars correspond to the upper and lower limits of viscosity at each RH from Song et al. [30]. Shown in blue are the viscosity predictions based on nano-DESI negative mode mass spectrometry results where it was assumed that the weight fraction of individual compounds was proportional to the mass spectrum signal intensity (eq 3). Shown in orange are the viscosity predictions where a relation between weight fraction and intensity given in eq 14 was assumed.

References

(1) Keywood, M. D.; Kroll, J. H.; Varutbangkul, V.; Bahreini, R.; Flagan, R. C.; Seinfeld, J. H. Secondary Organic Aerosol Formation from Cyclohexene Ozonolysis: Effect of OH Scavenger and the Role of Radical Chemistry. *Environ. Sci. Technol.* **2004**, *38* (12), 3343–3350. https://doi.org/10.1021/es049725j.

(2) Yonghui Shu; Atkinson, R. Atmospheric Lifetimes and Fates of a Series of Sesquiterpenes. *J. Geophys. Res.* **1995**, *100* (D4), 7275–7281. https://doi.org/10.1029/95JD00368.

(3) Baxley, J. S.; Wells, J. R. The Hydroxyl Radical Reaction Rate Constant and Atmospheric Transformation Products of 2-Butanol and 2-Pentanol. *Int. J. Chem. Kinet.* **1998**, *36* (10), 534–544. https://doi.org/10.1002/kin.20027.

(4) Seinfeld, J. H.; Pandis, S. N. *Atmospheric Chemistry and Physics*, 2nd Ed.; John Wiley and Sons: Hoboken, NJ, 2006.

(5) Price, H. C.; Mattsson, J.; Murray, B. J. Sucrose Diffusion in Aqueous Solution. *Phys. Chem. Chem. Phys.* **2016**, *18* (28), 19207–19216. https://doi.org/10.1039/C6CP03238A.

(6) Gorkowski, K.; Donahue, N. M.; Sullivan, R. C. Aerosol Optical Tweezers Constrain the Morphology Evolution of Liquid-Liquid Phase-Separated Atmospheric Particles. *Chem* **2020**, *6* (1), 204–220. https://doi.org/10.1016/j.chempr.2019.10.018.

(7) Hritz, A. D.; Raymond, T. M.; Dutcher, D. D. A Method for the Direct Measurement of Surface Tension of Collected Atmospherically Relevant Aerosol Particles Using Atomic Force Microscopy. *Atmos. Chem. Phys.* **2016**, *16* (15), 9761–9769. https://doi.org/10.5194/acp-16-9761-2016.

(8) Demond, A. H.; Lindner, A. S. Estimation of Interfacial Tension between Organic Liquids and Water. *Environ. Sci. Technol.* **1993**, *27* (12), 2318–2331. https://doi.org/10.1021/es00048a004.

(9) Gray Bé, A.; Upshur, M. A.; Liu, P.; Martin, S. T.; Geiger, F. M.; Thomson, R. J. Cloud Activation Potentials for Atmospheric α-Pinene and β-Caryophyllene Ozonolysis Products. *ACS Cent. Sci.* **2017**, *3* (7), 715–725. https://doi.org/10.1021/acscentsci.7b00112.

(10) Zhu, L.; Attard, P.; Neto, C. Reconciling Slip Measurements in Symmetric and Asymmetric Systems. *Langmuir* **2012**, *28* (20), 7768–7774. https://doi.org/10.1021/la301040d.

(11) Craig, V. S. J.; Neto, C.; Williams, D. R. M. Shear-Dependent Boundary Slip in an Aqueous Newtonian Liquid. *Phys. Rev. Lett.* **2001**, *87* (5), 54504-1-54504–4. https://doi.org/10.1103/PhysRevLett.87.054504.

(12) Baudry, J.; Charlaix, E.; Tonck, A.; Mazuyer, D. Experimental Evidence for a Large Slip Effect at a Nonwetting Fluid-Solid Interface. *Langmuir* **2001**, *17* (17), 5232–5236. https://doi.org/10.1021/la0009994.

(13) Tretheway, D. C.; Meinhart, C. D. Apparent Fluid Slip at Hydrophobic Microchannel Walls. *Phys. Fluids* **2002**, *14* (3). https://doi.org/10.1063/1.1432696.

(14) Joseph, P.; Tabeling, P. Direct Measurement of the Apparent Slip Length. *Phys. Rev. E - Stat. Nonlinear, Soft Matter Phys.* **2005**, *71* (3), 1–4. https://doi.org/10.1103/PhysRevE.71.035303.

(15) Churaev, N. V.; Sobolev, V. D.; Somov, A. N. Slippage of Liquids over Lyophobic Solid Surfaces. *J. Colloid Interface Sci.* **1984**, *97* (2), 574–581. https://doi.org/10.1016/0021-9797(84)90330-8.

(16) Vinogradova, O. I.; Koynov, K.; Best, A.; Feuillebois, F. Direct Measurements of Hydrophobic Slippage Using Double-Focus Fluorescence Cross-Correlation. *Phys. Rev. Lett.* **2009**, *102* (11), 1–5. https://doi.org/10.1103/PhysRevLett.102.118302.

(17) McBride, S. P.; Law, B. M. Viscosity-Dependent Liquid Slip at Molecularly Smooth Hydrophobic Surfaces. *Phys. Rev. E - Stat. Nonlinear, Soft Matter Phys.* **2009**, *80* (6), 2–5. https://doi.org/10.1103/PhysRevE.80.060601.

(18) Jing, D.; Bhushan, B. Boundary Slip of Superoleophilic, Oleophobic, and Superoleophobic Surfaces Immersed in Deionized Water, Hexadecane, and Ethylene Glycol. *Langmuir* **2013**, *29* (47), 14691–14700. https://doi.org/10.1021/la4030876.

(19) Cottin-Bizonne, C.; Jurine, S.; Baudry, J.; Crassous, J.; Restagno, F.; Charlaix, É. Nanorheology: An Investigation of the Boundary Condition at Hydrophobic and Hydrophilic Interfaces. *Eur. Phys. J. E* **2002**, *9* (1), 47–53. https://doi.org/10.1140/epje/i2001-10112-9.

(20) Cottin-Bizonne, C.; Cross, B.; Steinberger, A.; Charlaix, E. Boundary Slip on Smooth Hydrophobic Surfaces: Intrinsic Effects and Possible Artifacts. *Phys. Rev. Lett.* **2005**, *94* (5), 1–4. https://doi.org/10.1103/PhysRevLett.94.056102.

(21) Cho, J. H. J.; Law, B. M.; Rieutord, F. Dipole-Dependent Slip of Newtonian Liquids at Smooth Solid Hydrophobic Surfaces. *Phys. Rev. Lett.* **2004**, *92* (16), 1–4. https://doi.org/10.1103/PhysRevLett.92.166102.

(22) Bhushan, B.; Wang, Y.; Maali, A. Boundary Slip Study on Hydrophilic, Hydrophobic, and Superhydrophobic Surfaces with Dynamic Atomic Force Microscopy. *Langmuir* **2009**, *25* (14), 8117–8121. https://doi.org/10.1021/la900612s.

(23) Tasoglou, A.; Pandis, S. N. Formation and Chemical Aging of Secondary Organic Aerosol during the β -Caryophyllene Oxidation. *Atmos. Chem. Phys.* **2015**, *15*, 6035–6046. https://doi.org/10.5194/acp-15-6035-2015.

(24) Song, M. J.; Liu, P. F. F.; Hanna, S. J.; Zaveri, R. A.; Potter, K.; You, Y.; Martin, S. T.; Bertram, A. K. Relative Humidity-Dependent Viscosity of Secondary Organic Material from Toluene Photo-Oxidation and Possible Implications for Organic Particulate Matter over Megacities. *Atmos. Chem. Phys.* **2016**, *16* (14), 8817–8830. https://doi.org/10.5194/acp-16-8817-2016.

(25) Song, M.; Liu, P. F.; Hanna, S. J.; Li, Y. J.; Martin, S. T.; Bertram, A. K. Relative Humidity-Dependent Viscosities of Isoprene-Derived Secondary Organic Material and Atmospheric Implications for Isoprene-Dominant Forests. *Atmos. Chem. Phys.* **2015**, *15* (9), 5145–5159. https://doi.org/10.5194/acp-15-5145-2015.

(26) Grayson, J. W.; Zhang, Y.; Mutzel, A.; Renbaum-Wolff, L.; Böge, O.; Kamal, S.; Herrmann, H.; Martin, S. T.; Bertram, A. K. Effect of Varying Experimental Conditions on the Viscosity of α-Pinene Derived Secondary Organic Material. *Atmos. Chem. Phys.* **2016**, *16* (10), 6027–6040. https://doi.org/10.5194/acp-16-6027-2016.

(27) Crittenden, J. C.; Trussel, R. R.; Hand, D. W.; Howe, K. J.; Tchobanoglous, G. *MWH's Water Treatment*; John Wiley and Sons, 2012.

(28) DeRieux, W.-S. W.; Li, Y.; Lin, P.; Laskin, J.; Laskin, A.; Bertram, A. K.; Nizkorodov, S. A.; Shiraiwa, M. Predicting the Glass Transition Temperature and Viscosity of Secondary Organic

Material Using Molecular Composition. *Atmos. Chem. Phys.* **2018**, *18* (9), 6331–6351. https://doi.org/10.5194/acp-18-6331-2018.

(29) Hinks, M. L.; Montoya-Aguilera, J.; Ellison, L.; Lin, P.; Laskin, A.; Laskin, J.; Shiraiwa, M.; Dabdub, D.; Nizkorodov, S. A. Effect of Relative Humidity on the Composition of Secondary Organic Aerosol from the Oxidation of Toluene. *Atmos. Chem. Phys.* **2018**, *18* (3), 1643–1652. https://doi.org/10.5194/acp-18-1643-2018.

(30) Song, M.; Maclean, A. M.; Huang, Y.; Smith, N. R.; Blair, S. L.; Laskin, J.; Laskin, A.; DeRieux, W.-S. W.; Li, Y.; Shiraiwa, M.; Nizkorodov, S. A.; Bertram, A. K. Liquid-Liquid Phase Separation and Viscosity within Secondary Organic Aerosol Generated from Diesel Fuel Vapors. *Atmos. Chem. Phys.* **2019**, *19*, 12515–12529. https://doi.org/10.5194/acp-2019-367.